Chern Insulators at Integer and Fractional Filling in Moiré Pentalayer Graphene

Dacen Waters,[1,*] Anna Okounkova,[1,*] Ruiheng Su,[2,3] Boran Zhou,[4] Jiang Yao,[1] Kenji Watanabe,[5] Takashi Taniguchi,[6] Xiaodong Xu,[1,7] Ya-Hui Zhang,[4] Joshua Folk,[2,3] and Matthew Yankowitz[1,7,†]

[1]Department of Physics, University of Washington, Seattle, Washington 98195, USA
[2]Quantum Matter Institute, University of British Columbia, Vancouver, British Columbia, V6T 1Z1, Canada
[3]Department of Physics and Astronomy, University of British Columbia, Vancouver, British Columbia, V6T 1Z1, Canada
[4]Department of Physics and Astronomy, Johns Hopkins University, Baltimore, Maryland 21205, USA
[5]Research Center for Electronic and Optical Materials, National Institute for Materials Science, 1-1 Namiki, Tsukuba 305-0044, Japan
[6]Research Center for Materials Nanoarchitectonics, National Institute for Materials Science, 1-1 Namiki, Tsukuba 305-0044, Japan
[7]Department of Materials Science and Engineering, University of Washington, Seattle, Washington 98195, USA

(Received 12 November 2024; revised 7 January 2025; accepted 5 February 2025; published 27 February 2025)

The advent of moiré platforms for engineered quantum matter has led to discoveries of integer and fractional quantum anomalous Hall effects, with predictions for correlation-driven topological states based on electron crystallization. Here, we report an array of trivial and topological insulators formed in a moiré lattice of rhomobohedral pentalayer graphene (R5G). At a doping of one electron per moiré unit cell ($\nu = 1$), we see a correlated insulator with a Chern number that can be tuned between $C = 0$ and $+1$ by an electric displacement field. This is accompanied by a series of additional Chern insulators with $C = +1$ originating from fractional fillings of the moiré lattice—$\nu = 1/4$, $1/3$, and $2/3$—associated with the formation of moiré-driven topological electronic crystals. At $\nu = 2/3$ the system exhibits an integer quantum anomalous Hall effect at zero magnetic field, but further develops hints of an incipient $C = 2/3$ fractional Chern insulator in a modest field. Our results establish moiré R5G as a fertile platform for studying the competition and potential intertwining of integer and fractional Chern insulators.

DOI: 10.1103/PhysRevX.15.011045 Subject Areas: Condensed Matter Physics, Materials Science

I. INTRODUCTION

Moiré materials with flat bands are ideal platforms for studying the interplay between strongly correlated and topological states of matter [1–5]. Early work in this field established the existence of a wide range of correlation-driven topological states within the magnetic subbands of the Hofstadter butterfly spectrum, including states that break the translational symmetry of the moiré lattice (called "symmetry-broken Chern insulators") and others featuring fractionalized quasiparticles [fractional Chern insulators (FCI)] [6,7]. Recently, remarkable progress has been made in achieving analogous states in the absence of an external magnetic field using moiré lattices with flat bands and suitable topological properties. Prominent examples include the integer and fractional quantum anomalous Hall (IQAH and FQAH) states found in twisted bilayer $MoTe_2$ [8–11] and rhombohedral multilayer graphene aligned with hexagonal boron nitride (h-BN) [12–14], as well as Chern insulator states with discrete translational symmetry breaking found in several twisted graphene structures [15–17].

Forming Chern insulators in moiré lattices requires spontaneous valley polarization, resulting in broken time-reversal symmetry [4,5]. Many-body gaps can be opened at integer fillings of the moiré flat bands, resulting in the IQAH effect when the filled bands have nonzero total Chern number. Topological gapped states can also form at fractional fillings of the moiré bands, but require the assistance of additional correlation-driven mechanisms. FQAH states are a notable example, forming anyonic quasiparticles but otherwise not needing to break any of the remaining symmetries of the system. Alternatively,

*These authors contributed equally to this work.
†Contact author: myank@uw.edu

electrons can spontaneously break translational symmetry to form topological electronic crystal (TEC) states exhibiting an IQAH effect. Examples include the anomalous Hall crystal, recently considered for moiré and nonmoiré rhombohedral pentalayer graphene (R5G) [18–28], and moiré-driven topological electronic crystals in other twisted graphene lattices [15–17]. Understanding the interplay between integer and fractional QAH states at fractional band filling presents a critical open challenge for the field.

Here, we study an array of correlated insulating states arising in a moiré lattice of R5G aligned to h-BN, with a period of 10.8 nm. Recent pioneering work on this system revealed the emergence of FQAH states at several Jain-sequence fractions for $\nu < 1$, all arising in a device with a slightly larger moiré period of 11.5 nm [13]. In contrast, our device instead exhibits IQAH states originating from both integer and fractional fillings of the electron-doped moiré conduction band. The insulating states are most robust near commensurate band fillings ($\nu = 4n/n_s = 1/3$, $2/3$, and 1, where n_s is the moiré superlattice density [29]), but nevertheless extend over a wide range of moiré band filling, $0 < \nu \lessapprox 1$. In a magnetic field, there are signatures of both integer and fractional Chern insulators associated with $\nu = 2/3$. A second device, with an even smaller (8.8 nm) moiré period, does not exhibit any such correlated insulators at commensurate band fillings, further hinting at the key role of the moiré potential in generating these states (see Supplemental Material and Fig. S18 [29]).

II. TRIVIAL AND TOPOLOGICAL CORRELATED INSULATORS

Figure 1(a) shows a schematic of our device, in which R5G is nearly aligned to one h-BN dielectric but misaligned from the other. The top and bottom graphite gates enable independent control over n and D, the latter of which we define to be positive when available states in the conduction band are pushed away from the moiré interface. Figure 1(b) shows a map of the longitudinal resistance ρ_{xx} of the device taken over a wide range of n and D. We extract the density needed to fully fill the lowest moiré bands ($\nu = \pm 4$) to be $n_s = 3.98 \times 10^{12}$ cm^{-2}, corresponding to a moiré period of 10.8 nm and a twist angle between the R5G and h-BN of $\theta = 0.90°$ (assuming a 1.7% lattice mismatch between graphene and h-BN). Overall, the salient features we see are consistent with those reported in a prior study of moiré R5G [13], including a series of insulating states at the charge neutrality point ($\nu = 0$) and resistive states at various integer values of ν corresponding to either correlated or single-particle band insulators [29].

Figure 1(c) shows a continuum model band structure calculation for an interlayer potential difference of $\delta = +150$ meV [29]. The calculation predicts that the lowest moiré conduction band (colored in purple) is gapped from the highest moiré valence band, but overlaps the second conduction band. Both of these features are consistent with the experiment, in which there is an insulating state at $\nu = 0$ but a metallic state at $\nu = 4$ for large positive D [see Fig. 1(d) for a representative measurement at $D = 0.740$ V/nm, corresponding to the purple dashed line in Fig. 1(b)].

Figures 1(e) and 1(f) show enlarged maps of the field-symmetrized longitudinal (ρ_{xx}) and antisymmetrized Hall (ρ_{xy}) resistances in the high-D region between $\nu = 0$ and $\nu \approx 1$, outlined by the black dashed square in Fig. 1(b). The key features seen in these maps are summarized in Fig. 1(g). Most obviously, a stripelike region cuts diagonally across the center of the maps in Figs. 1(e) and 1(f), in which one or both of ρ_{xx} and ρ_{xy} are very large. The system is a trivial insulator for $\nu \lessapprox 1/2$–$2/3$ (depending on the precise value of D), previously attributed to the formation of a Wigner crystal with period larger than the original moiré lattice [13]. There is also a pocket centered at $\nu = 2/3$ featuring large ρ_{xy} and a deep suppression of ρ_{xx}. This behavior instead indicates the formation of a topological gapped state. Finally, there is a vertical feature at $\nu = 1$ that exhibits a large anomalous Hall effect (AHE) for D larger than a critical value of $D_c \approx 0.82$ V/nm, but diverging ρ_{xx} with no AHE for $D < D_c$ [Figs. 1(h) and 1(i)].

III. TOPOLOGICAL PHASE TRANSITION AT $\nu = 1$

To probe the nature of these states, we plot Landau fan diagrams for two values of displacement field [Figs. 2(a) and 2(b)]. At $D = 0.910$ V/nm, we see a correlated Chern insulator emerging from $B = 0$ at $\nu = 1$, along with additional associated quantum Hall states to its right at higher field. A line cut at $B = 0.75$ T in Fig. 2(c) confirms that the correlated Chern insulator state exhibits the anticipated values of $\rho_{xx} \approx 0$ and $\rho_{xy} \approx h/e^2$, where h is Planck's constant and e is the charge of the electron. Comparison to the Streda formula [30,31], $(\partial n/\partial B) = C(h/e)$, further indicates that the Chern number of this state is $C = +1$ (see the white dashed line at the top of the Landau fans). We label gapped states by their Chern number and band filling upon extrapolation to $B = 0$ following the convention $(C = a, \nu = b) \equiv C_b^a$, such that this state is C_1^{+1}.

The Landau fan taken at $D = 0.740$ V/nm exhibits markedly different behavior. At $\nu = 1$, ρ_{xx} far exceeds h/e^2 and ρ_{xy} exhibits diverging behavior with an abrupt sign reversal across integer filling [see line cuts in Fig. 2(d) taken at $B = 0.20$ T]. The insulating state does not disperse with B, and associated quantum Hall states emerge roughly symmetrically to its left and right. Collectively, this behavior is consistent with a topologically trivial state C_1^0. Apparently, the critical displacement field, $D_c \approx 0.82$ V/nm, where the AHE at $\nu = 1$ vanishes corresponds to a phase transition between two topologically distinct states with associated Chern numbers of $C = 0$ and $+1$. Such a phase transition typically requires

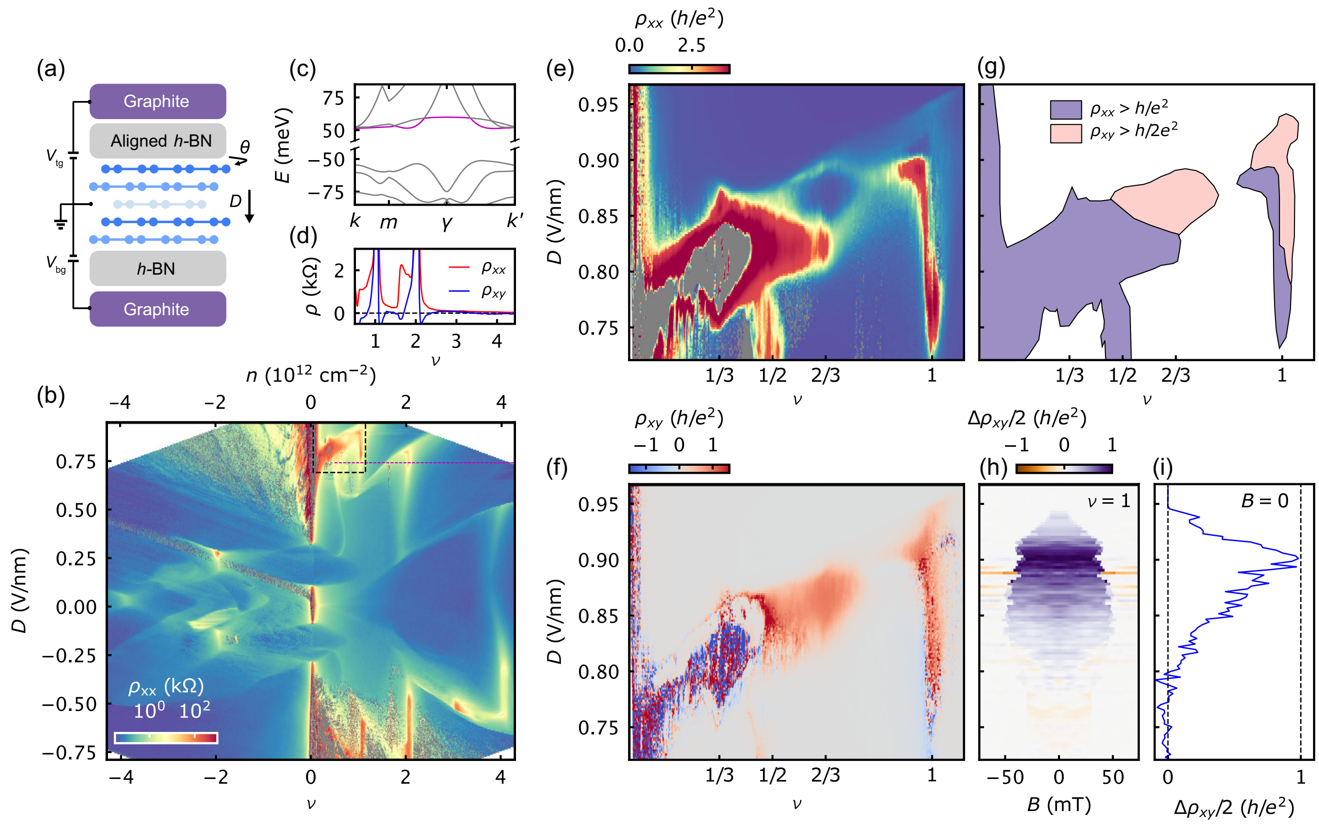

FIG. 1. Device transport characterization and correlated states at $\nu \le 1$. (a) Schematic of the device. R5G is encapsulated between flakes of h-BN with graphite top and bottom gates. The R5G is misaligned from the bottom h-BN, and has a small twist angle of $\theta = 0.90°$ with the top h-BN to form a moiré superlattice [29]. (b) Map of ρ_{xx} taken at $B = 0$ over a wide range of the $n - D$ parameter space. The data are acquired in multiple submeasurements to mitigate measurement artifacts [29]. The gray colored data in the color scale indicate that ρ_{xx} was measured to be negative, indicating either a highly resistive state or poor equilibration of the contacts [29]. (c) Single-particle calculated band structure with $\delta = +150$ meV and a moiré period of 10.8 nm. This sign of δ corresponds to $D > 0$. The lowest moiré conduction band is colored in purple. (d) Line traces of ρ_{xx} and ρ_{xy} acquired at $D = 0.740$ V/nm [corresponding to the position of the purple dashed line in (b)] with $B = 0.2$ T (not symmetrized). (e) Enlarged map of ρ_{xx} symmetrized at $|B| = 100$ mT from the region of the black dashed box in (b). (f) Similar map of antisymmetrized ρ_{xy}. (g) Schematic indicating transport features seen in (e) and (f). Regions shaded in pink satisfy the condition $\rho_{xy} > h/2e^2$. Regions shaded in purple satisfy the condition $\rho_{xx} > h/e^2$. Regions satisfying both conditions are also shaded in purple (since the large value of ρ_{xy} is an artifact corresponding to mixing with ρ_{xx}). Regions with negative ρ_{xx} are shaded in purple, as they correspond to measurement artifacts in very insulating states [29]. (h) Map of $\Delta\rho_{xy}/2 = (\rho_{xy}^{\uparrow} - \rho_{xy}^{\downarrow})/2$ at $\nu = 1$, where the arrows indicate the direction B is swept. (i) A line cut of $\Delta\rho_{xy}/2$ from (h) at $B = 0$.

a gap closure and reopening; we do not see evidence for this in our device, potentially due to disorder.

Many recent theory works [18–20,22–28,32,33] have considered the nature of the Chern insulator previously reported at $\nu = 1$ [13] in R5G aligned to h-BN. In many other moiré systems, a correlated gap opens at $\nu = 1$ when the fourfold isospin degeneracy is lifted by interactions [4,5]. But in R5G, the second moiré conduction band overlaps the first; as a result, this mechanism alone would not be expected to open a gap. Instead, the additional formation of a topological electronic crystalline order via a large spatial redistribution of the charge density is believed to open the gap [18–28]. However, a definitive understanding of the gap at $\nu = 1$ remains elusive because the putative electronic crystal is commensurate with the moiré lattice, and is thus challenging to distinguish unambiguously from conventional moiré Chern insulators [34]. Nevertheless, the basic TEC framework is consistent with the $C = 1$ state we observe at $\nu = 1$. The trivial $C = 0$ insulator at smaller D can be formed similarly by lifting the same isospin degeneracies and crystallizing the electrons, but needs the filled states to instead have a total Chern number of zero.

To better understand the possible nature of the gapped states at $\nu = 1$, we compare our results to Hartree-Fock (HF) calculations performed in a simplified model where the moiré potential is artificially set to zero (more realistic calculations with nonzero moiré potential yield similar conclusions; see Ref. [29]). Figures 2(e) and 2(f) show the calculated band structure at $\nu = 1$ both with and without

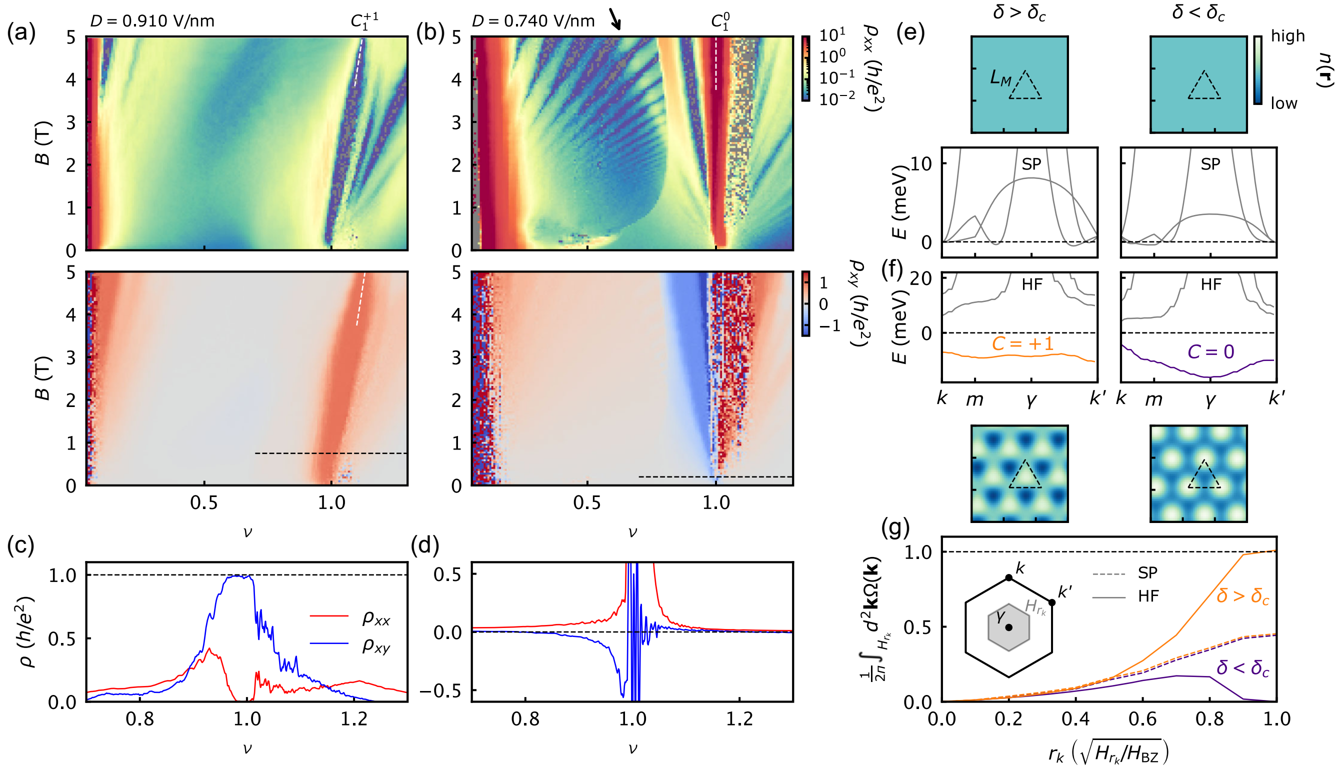

FIG. 2. Topological and trivial correlated insulators at $\nu = 1$. (a) Landau fan diagram of ρ_{xx} (top) and ρ_{xy} (bottom) taken at $D = 0.910$ V/nm. The white dashed line shows the expected evolution of a $C = +1$ state originating from $\nu = 1$ based on the Streda formula. (b) Similar Landau fan taken at $D = 0.740$ V/nm. The white dashed line shows the expected evolution of a $C = 0$ state originating from $\nu = 1$. The black arrow denotes the trajectory of a quantum Hall state with filling factor of -3 originating from $\nu = 1$. The speckled features projecting vertically near $\nu = 1$ are artifacts due to a large contact resistance. (c) Line traces of ρ_{xx} and ρ_{xy} taken at $B = 0.75$ T from the $D = 0.910$ V/nm Landau fan, as indicated by the black dashed line in (a). (d), Similar line cuts taken at $B = 0.20$ T from the $D = 0.740$ V/nm Landau fan, as indicated by the black dashed line in (b). (e) Single-particle (SP) calculations of the spatial distribution of carrier density $n(\mathbf{r})$ at a filling of $\nu = 1$. The left-hand (right-hand) panel is calculated with $\delta = 150$ meV (120 meV). Both correspond to metallic states. The associated band structure calculations are shown below each plot. The calculation is performed for a moiré period of $L_M = 11.1$ nm with the moiré potential strength artificially set to zero [29]. (f) Similar calculations performed with the Hartree-Fock (HF) method. Both correspond to insulating states, with the filled band having $C = +1$ (0) for $\delta = 150$ meV (120 meV), shown in orange (purple). Dashed lines at zero energy in (e) and (f) denote the Fermi energy at $\nu = 1$. The real-space densities in (e) and (f) share the same color scale. The dashed black triangles indicate the moiré unit cell. (g) Berry curvature integrated from the center to the edge of the moiré Brillouin zone (BZ) for both values of δ considered in (e) and (f). The dashed (solid) curves show the single-particle (Hartree-Fock) calculations. The inset schematic shows the moiré BZ in black, with high symmetry points labeled. The gray area depicts the area of integration, which scales with r_k, such that $H_{r_k} = r_k^2 H_{\mathrm{BZ}}$, where H_{BZ} is the area of the full moiré BZ.

the HF approximation for two different values of δ. In both cases, the state is gapless at the single-particle level but gapped as a result of interactions. The isolated band has a Chern number of $C = 0$ for δ less than a critical value of $\delta_c \approx 140$ meV, but $C = +1$ for $\delta > \delta_c$. This is consistent with our observed phase transition between a $C = 0$ and $+1$ state as D is increased. At the noninteracting level, the integrated Berry curvature up to the Fermi level at $\nu = 1$ can be any arbitrary value since the band is not isolated. Figure 2(g) shows that this value is $(1/2\pi)\int_{\mathrm{BZ}} d^2\mathbf{k}\Omega(\mathbf{k}) \approx 0.5$ in the calculations for both $\delta = 120$ and 150 meV [29]. When interactions open a gap, however, the filled states below the Fermi level must have Berry curvature that integrates to a quantized value, equal to C. In this context, the gap opening simultaneously necessitates an interaction-driven modification of the Berry curvature in order to satisfy the quantization condition. Small changes in the quantum geometry of the single-particle bands with δ can thus lead to an abrupt phase transition between otherwise similar states having $C = 0$ (e.g., a generalized Wigner crystal [35]) and $C = 1$ (e.g., a moiré-driven TEC [17]).

IV. INTEGER AND FRACTIONAL CHERN INSULATORS AT $\nu = 2/3$

Next we turn to the topological states observed at fractional band filling in Figs. 1(e) and 1(f). Figure 3(a) shows a Landau fan acquired at $D = 0.863$ V/nm, which cuts through a region with a ρ_{xx} minimum and concomitant $\rho_{xy} \approx h/e^2$ surrounding $\nu = 2/3$ [see line cuts in Fig. 3(b)]. Sweeping the perpendicular magnetic field at $\nu = 2/3$, ρ_{xy} switches between $\approx \pm h/e^2$ in a single hysteresis loop with a small coercive field of $B \approx 10$ mT [Fig. 3(c)]. The slope of this state in the Landau fan is consistent with a $C = +1$ Chern insulator based on the Streda formula (i.e., $C^{+1}_{2/3}$), as indicated by the black dashed line in Fig. 3(a). These features are plainly incompatible with the $C = 2/3$ FQAH state at $\nu = 2/3$ reported previously [13], since our observed state has neither the appropriate Streda slope in the Landau fan nor the appropriate quantization of ρ_{xy} for a $C = 2/3$ state (that is, we find $\rho_{xy} = h/e^2$ rather than $3h/2e^2$). Instead, the gapped $C^{+1}_{2/3}$ state most naturally corresponds to a moiré-driven TEC that spontaneously enlarges the unit cell area [29]. Notably, ρ_{xy} remains large over a relatively wide range of doping, potentially indicating that the crystalline order persists in some form even upon doping away from $\nu = 2/3$.

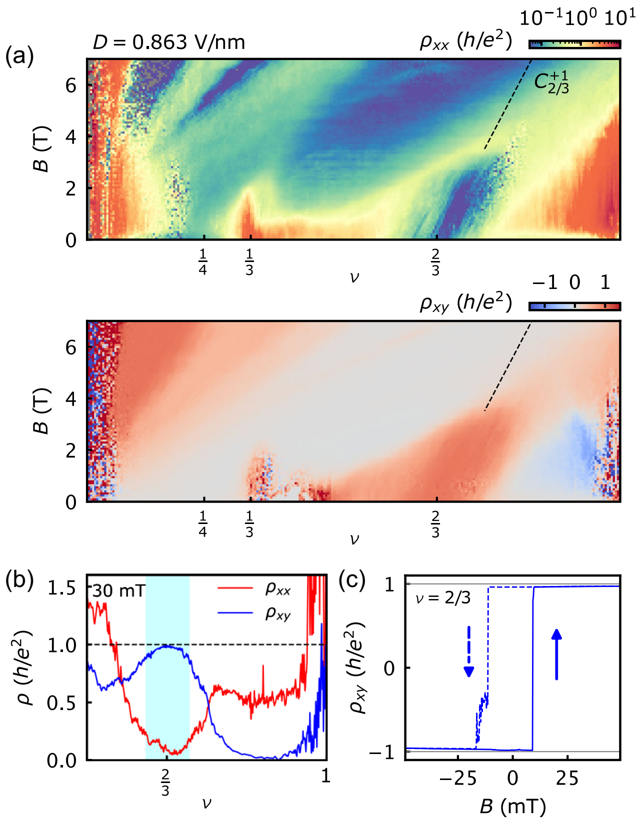

FIG. 3. IQAH state at $\nu = 2/3$. (a) Landau fan diagram of ρ_{xx} (top) and ρ_{xy} (bottom) taken at $D = 0.863$ V/nm. The black dashed line shows the expected evolution of a $C = +1$ state originating from $\nu = 2/3$ based on the Streda formula. (b) Line traces of ρ_{xx} and ρ_{xy} taken at $B = 30$ mT from the $D = 0.863$ V/nm Landau fan in (a). The blue shaded region corresponds to the contiguous range of ν for which $\rho_{xy} > 0.9h/e^2$. (c) Measurement of ρ_{xy} at $\nu = 2/3$ acquired as B is swept back and forth across zero. Arrows denote the sweep direction of the magnetic field.

Figure 4(a) shows a Landau fan at $D = 0.820$ V/nm, which differs at zero and small B in that it is dominated by a trivial insulating state. However, a series of topological states abruptly emerge above $B \approx 2$ T, including three $C = +1$ states projecting to $\nu = 1/4$, $1/3$, and $2/3$ at $B = 0$. These also correspond to moiré-driven TEC states with associated unit-cell enlargement, but require the assistance of the magnetic field to form [see line cuts in Figs. 4(b)–4(d)]. Additionally, there is an oval-shaped feature near $\nu \approx 0.6$ centered at $B \approx 3.5$ T, in which both ρ_{xx} and ρ_{xy} are abruptly suppressed and there are instead quantum Hall states projecting to the charge neutrality point at $\nu = 0$. This region is separated from the surrounding area of the Landau fan by a first-order phase transition and has the same origin as the sharp curved feature in the Landau fan in Fig. 2(b). This phase transition potentially reflects a collapse of the crystalline electronic order [29].

Remarkably, the Landau fan also contains an extremely narrow feature in which the antisymmetrized ρ_{xy} clearly exceeds h/e^2 [see the line cut in Fig. 4(e)]. The purple dashed line near the top of the Landau fan denotes the position and trajectory of this state, which projects precisely to $\nu = 2/3$ at $B = 0$ and has a Streda slope matching a $C = +2/3$ state (i.e., $C^{+2/3}_{2/3}$). These features are consistent with an incipient $\nu = 2/3$ FCI state emerging with B. Although the state is not fully developed, with large residual ρ_{xx} and nonquantized ρ_{xy}, the observation of $\rho_{xy} > h/e^2$ with a Streda slope implying $C = +2/3$ has no simple explanation besides a field-induced FCI state.

V. DISCUSSION

Our measurements reveal two unexpected new features of moiré R5G. First, we find that the correlated insulator at $\nu = 1$ can have a Chern number of either $C = 0$ or 1, depending on D. Although the nature of these two states remains to be fully understood, the existence of the $C = 0$ insulator sharply constrains potential theoretical descriptions of the system. We have considered a possible model in which the many-body gap opening simultaneously drives a substantial redistribution of Berry curvature, with small changes in the interlayer potential tipping the balance of the filled band toward either $C = 0$ or 1. These two states are predicted to feature different real-space charge distributions [Fig. 2(f)], which may be detectable in future scanning probe experiments.

Second, we find that the correlated state at $\nu = 2/3$ can exhibit an IQAH with $C = 1$, rather than the previously observed FQAH with $C = 2/3$ [13]. Such a state is most naturally explained by a spontaneous enlargement of the unit cell, corresponding to the formation of a Chern insulator at integer filling of the folded Brillouin zone.

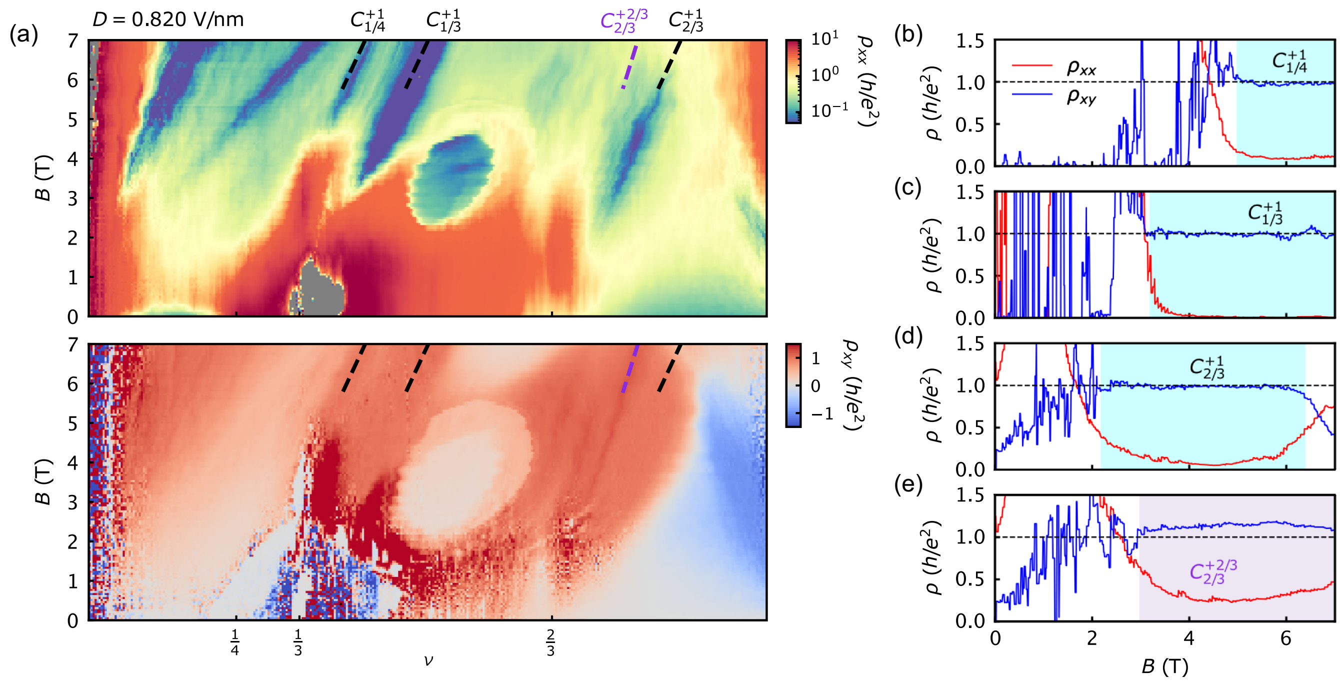

FIG. 4. Integer and fractional Chern insulators at fractional ν. (a) Landau fan of ρ_{xx} (top) and ρ_{xy} (bottom), taken at $D = 0.820$ V/nm. The black dashed lines show the expected evolution of $C = +1$ states originating from $\nu = 1/4$, $1/3$, and $2/3$. The purple dashed line shows the same for a $C = +2/3$ state originating from $\nu = 2/3$. (b) Line traces of ρ_{xx} and ρ_{xy} taken along the trajectory indicated by the black dashed line associated with the $C^{+1}_{1/4}$ state in (a). The blue shaded region corresponds to the contiguous region of $|\rho_{xy}| > 0.9h/e^2$ (excluding $B < 4.5$ T which is dominated by the trivial insulating phase). (c),(d) Similar line traces and shading for the $C^{+1}_{1/3}$ and $C^{+1}_{2/3}$ states in (a),(c). (e) Similar line traces taken along the trajectory indicated by the purple dashed line associated with the $C^{+2/3}_{2/3}$ state in (a). The purple shaded region corresponds to contiguous range of ν for which $\rho_{xy} > h/e^2$ (excluding $B < 3$ T).

Hints of the $C = 2/3$ FCI state additionally appear once a few-Tesla magnetic field is applied, pointing to a close competition between the integer and fractional Chern insulator states. The appearance of both states in a magnetic field is possible because these two states bifurcate to different values of charge doping with B, as described by the Streda formula, and can thus be stabilized separately by gating.

Our results highlight the need for additional experiments to map out the dependence of FQAH and electronic crystal states on the precise value of the moiré period, as well as other device parameters such as strain and Coulomb screening [36]. As a first step in this direction, we show measurements from a second device with a slightly larger twist angle, and thus a smaller moiré period of 8.8 nm, in Supplemental Material [29]. Although many of the salient transport features resemble those observed in Fig. 1(b), there are no correlated insulators at any integer or rational fractional values of ν for any D [29]. The absence of such states provides evidence that a long-wavelength moiré potential may be necessary for seeding the formation of integer and fractional QAH states in R5G. Understanding the sensitive dependence of these states on twist angle may help to unravel the nature of the rich correlated phase diagram of moiré R5G.

Looking forward, scanning probe studies will be crucial for directly imaging the putative charge-ordered states in this system, enabling a better understanding of the nature of the doping–and displacement field–dependent translational symmetry breaking. Such measurements will also be helpful for determining the potential effects of disorder, which may localize charge or create defects in the electronic crystalline states. Understanding the relationship between integer and fractional Chern insulators also stands as a critical open challenge for the field, especially as it relates to determining the ultimate ground state ordering of the system.

ACKNOWLEDGMENTS

The authors thank Long Ju for sharing preliminary data; Hart Goldman, Trithep Devakul, and David Cobden for helpful discussions; and Yinong Zhang, Jordan Fonseca, and Jiaqi Cai for technical assistance with the AM-KPFM imaging of graphene stacking domains. Research at the University of Washington on correlation-driven topology in pentalayer graphene was solely supported as part of Programmable Quantum Materials, an Energy Frontier Research Center funded by the U.S. Department of Energy (DOE), Office of Science, Basic Energy Sciences

(BES), under Award No. DE-SC0019443. Experiments at the University of British Columbia were undertaken with support from the Natural Sciences and Engineering Research Council of Canada; the Canada Foundation for Innovation; the Canadian Institute for Advanced Research; the Max Planck-UBC-UTokyo Centre for Quantum Materials and the Canada First Research Excellence Fund, Quantum Materials and Future Technologies Program; and the European Research Council (ERC) under the European Union's Horizon 2020 research and innovation program, Grant Agreement No. 951541. D. W. was supported by the Intelligence Community Postdoctoral Research Fellowship Program at University of Washington administered by Oak Ridge Institute for Science and Education through an interagency agreement between the U.S. Department of Energy and the Office of the Director of National Intelligence. M. Y., X. X., and A. O. acknowledge support from the State of Washington-funded Clean Energy Institute. K. W. and T. T. acknowledge support from the JSPS KAKENHI (Grants No. 21H05233 and No. 23H02052) and World Premier International Research Center Initiative (WPI), MEXT, Japan. This work made use of shared fabrication facilities at UW provided by NSF MRSEC 2308979 with graphene device development supported by National Science Foundation (NSF) CAREER Award No. DMR-2041972. Theoretical calculations were supported by the National Science Foundation under Grant No. DMR-2237031. This work acknowledges usage of the millikelvin optoelectronic quantum material laboratory supported by the M. J. Murdock Charitable Trust.

A. O. and D. W. developed the sample fabrication capabilities; A. O. fabricated the sample; D. W. and A. O. measured the sample in the Yankowitz lab at UW; R. S. performed follow-up measurements in the Folk lab at UBC, which appear in many of the main text figures, under the supervision of J. F. and in discussion with D. W., A. O., and M. Y.; D. W. and A. O analyzed the data with the assistance of R. S.; J. Y. developed the atomic force microscopy-based imaging technique to detect rhombohedral graphene under the supervision of X. X.; M. Y. supervised the project; D. W., A. O, and M. Y. wrote the manuscript with B. Z. and Y.-H. Z. providing theory support; K. W. and T. T. provided the *h*-BN crystals.

The authors declare no competing interests.

DATA AVAILABILITY

All data that support the findings of this study are available from the contact author upon request.

[1] L. Balents, C. R. Dean, D. K. Efetov, and A. F. Young, *Superconductivity and strong correlations in moiré flat bands*, Nat. Phys. **16**, 725 (2020).

[2] E. Y. Andrei and A. H. MacDonald, *Graphene bilayers with a twist*, Nat. Mater. **19**, 1265 (2020).

[3] K. F. Mak and J. Shan, *Semiconductor moiré materials*, Nat. Nanotechnol. **17**, 686 (2022).

[4] K. P. Nuckolls and A. Yazdani, *A microscopic perspective on moiré materials*, Nat. Rev. Mater. **9**, 460 (2024).

[5] P. C. Adak, S. Sinha, A. Agarwal, and M. M. Deshmukh, *Tunable moiré materials for probing Berry physics and topology*, Nat. Rev. Mater. **9**, 481 (2024).

[6] C. R. Dean *et al.*, *Hofstadter's butterfly and the fractal quantum Hall effect in moiré superlattices*, Nature (London) **497**, 598 (2013).

[7] E. M. Spanton *et al.*, *Observation of fractional Chern insulators in a van der Waals heterostructure*, Science **360**, 62 (2018).

[8] J. Cai *et al.*, *Signatures of fractional quantum anomalous Hall states in twisted* $MoTe_2$, Nature (London) **622**, 63 (2023).

[9] Y. Zeng *et al.*, *Thermodynamic evidence of fractional Chern insulator in moiré* $MoTe_2$, Nature (London) **622**, 69 (2023).

[10] H. Park *et al.*, *Observation of fractionally quantized anomalous Hall effect*, Nature (London) **622**, 74 (2023).

[11] F. Xu *et al.*, *Observation of integer and fractional quantum anomalous Hall effects in twisted bilayer* $MoTe_2$, Phys. Rev. X **13**, 031037 (2023).

[12] G. Chen *et al.*, Tunable correlated Chern insulator and ferromagnetism in a moiré superlattice. Nature (London) **579**, 56 (2020).

[13] Z. Lu *et al.*, *Fractional quantum anomalous Hall effect in multilayer graphene*, Nature (London) **626**, 759 (2024).

[14] J. Xie *et al.*, *Even- and odd-denominator fractional quantum anomalous Hall effect in graphene moiré superlattices*, arXiv:2405.16944.

[15] Y. Xie *et al.*, *Fractional Chern insulators in magic-angle twisted bilayer graphene*, Nature (London) **600**, 439 (2021).

[16] H. Polshyn *et al.*, *Topological charge density waves at half-integer filling of a moiré superlattice*, Nat. Phys. **18**, 42 (2022).

[17] R. Su, D. Waters, B. Zhou, K. Watanabe, T. Taniguchi, Y.-H. Zhang, M. Yankowitz, and J. Folk, *Moiré-driven topological electronic crystals in twisted graphene*, Nature (London) **637**, 1084 (2025).

[18] Z. Dong, A. S. Patri, and T. Senthil, *Theory of fractional quantum anomalous Hall phases in pentalayer rhombohedral graphene moiré structures*, Phys. Rev. Lett. **133**, 206502 (2024).

[19] B. Zhou, H. Yang, and Y. Zhang, *Fractional quantum anomalous Hall effects in rhombohedral multilayer graphene in the moiréless limit*, Phys. Rev. Lett. **133**, 206504 (2024) (2023).

[20] J. Dong *et al.*, *Anomalous Hall crystals in rhombohedral multilayer graphene I: Interaction-driven Chern bands and fractional quantum Hall states at zero magnetic field*, Phys. Rev. Lett. **133**, 206503 (2024).

[21] Y. H. Kwan, J. Yu, J. Herzog-Arbeitman, D. K. Efetov, N. Regnault, and B. A. Bernevig, *Moiré fractional Chern*

insulators III: Hartree-Fock phase diagram, magic angle regime for Chern insulator states, the role of the moiré potential and Goldstone gaps in rhombohedral graphene superlattices, arXiv:2312.11617.

[22] T. Tan and T. Devakul, *Parent Berry curvature and the ideal anomalous Hall crystal*, Phys. Rev. X **14**, 041040 (2024).

[23] T. Soejima *et al.*, *Anomalous Hall crystals in rhombohedral multilayer graphene II: General mechanism and a minimal model*, Phys. Rev. B **110**, 205124 (2024).

[24] Z. Dong, A. S. Patri, and T. Senthil, *Stability of anomalous Hall crystals in multilayer rhombohedral graphene*, Phys. Rev. B **110**, 205130 (2024).

[25] X. Shen *et al.*, *Stabilizing fractional Chern insulators via exchange interaction in moiré systems*, arXiv:2405.12294.

[26] Y. Zeng, D. Guerci, V. Crepel, A. J. Millis, and J. Cano, *Sublattice structure and topology in spontaneously crystallized electronic states*, Phys. Rev. Lett. **132**, 236601 (2024).

[27] K. Kudo, R. Nakai, and K. Nomura, *Quantum anomalous, quantum spin, and quantum valley Hall effects in pentalayer rhombohedral graphene*, Phys. Rev. B **110**, 245135 (2024).

[28] V. Crépel and J. Cano, *Efficient prediction of superlattice and anomalous miniband topology from quantum geometry*, Phys. Rev. X **15**, 011004 (2025).

[29] See Supplemental Material at http://link.aps.org/supplemental/10.1103/PhysRevX.15.011045, which includes methods, Supplemental Text, and Supplemental Figs. 1–18.

[30] P. Streda, *Quantised Hall effect in a two-dimensional periodic potential*, J. Phys. C **15**, L1299 (1982).

[31] P. Streda, *Theory of quantised Hall conductivity in two dimensions*, J. Phys. C **15**, L717 (1982).

[32] J. Yu, J. Herzog-Arbeitman, Y. H. Kwan, N. Regnault, and B. A. Bernevig, *Moiré fractional Chern insulators IV: Fluctuation-driven collapse of FCIs in multi-band exact diagonalization calculations on rhombohedral graphene*, arXiv:2407.13770.

[33] K. Huang, S. Das Sarma, and X. Li, *Fractional quantum anomalous Hall effect in rhombohedral multilayer graphene with a strong displacement field*, arXiv:2408.05139 [Phys. Rev. B (to be published)].

[34] S. A. Parameswaran, *Anomalous Hall crystals or moiré Chern insulators? Spontaneous versus explicit translational symmetry breaking in graphene pentalayers*, J. Club Condens. Matter Phys. (2024).10.36471/JCCM_January_2024_02

[35] E. C. Regan *et al.*, *Mott and generalized Wigner crystal states in* WSe_2/WS_2 *moiré superlattices*, Nature (London) **579**, 359 (2020).

[36] X. Liu *et al.*, *Tuning electron correlation in magic-angle twisted bilayer graphene using Coulomb screening*, Science **371**, 1261 (2021).